Journal Name

ARTICLE

Synthesis and photophysical characterization of dimethylamine-derived Zn(II)Phthalocyanines: exploring their potential as selective chemosensors for trinitrophenol

N. Venkatramaiah,[a,b] Deisy M. G. C. Rocha,[a] P. Srikanth,[c] Filipe A. Almeida Paz[b*] and João P. C. Tomé[a,d*]

We report a novel synthetic approach, with good yields, for the synthesis of selective dimethylamine-substituted phthalonitriles (**1-3**) in the presence of triethyl phosphite and dimethylformamide at 160 $^\circ$C. The peripherally-modified dimethylamine substituted Zn(II)phthalocyanines (**ZnPc1-3**) with varied number and position of dimethylamine groups were prepared for a systematic investigation on the effect of the substituents on their electronic and spectroscopic properties. Compounds show strong aggregation behaviour in methanol and this behaviour decreasing with the increase of the alkyl chain of the alcohol solvents (*i.e.*, from methanol to octanol). The fluorescence quantum yields of **ZnPc1-3** showed an excellent correlation with the extent of the molecular aggregation. The versatility of the **ZnPc1-5** compounds possessing both electron donating and electron withdrawing substituents at their periphery is investigated towards the detection of nitroaromatic compounds (NACs) in solution and in the vapour phase. It was found that **ZnPc1-5** exhibit high selectivity towards trinitrophenol (TNP). A good linearity of the fluorescence detection using **ZnPc3** as the fluorescent probe was observed in the concentration range of 50×10^{-6}–450×10^{-6} M in chloroform, with a detection limit (LOD) of 11±2 ppm. Stern-Volmer (SV) and DFT studies reveal that the fluorescence quenching behaviour occurs through photo-induced electron transfer from the excited state of **ZnPcs** to TNP with static quenching behaviour occurring in a predominant fashion. The formation of porous morphology of **ZnPc3** thin film promotes high selectivity and accessibility to TNP vapours (7.7×10^{-3} ppb).

1.Introduction

Considerable interest has recently been focused in the design of stimuli-responsive smart materials with tuneable photophysical properties. Phthalocyanines (Pcs) and related cyclic tetrapyrrolic macrocycles comprise a highly conjugated π-electron family that exhibit strong absorption of light in the 600-700 nm spectral.[1,2] In this sense, the unique optical properties of these compounds are explored in different applications acting as functional materials.[3] The low solubility of un-substituted phthalocyanine in organic solvents or water limits, however, their practical application. Hence, a number of phthalocyanine derivatives have been synthesized bearing modified peripheral substituents with π-conjugation and with a wide range of functional groups so to enhance its solubility.[4-6] Various metal ions can also be inserted at the central core of the ring resulting in the formation of metallophthalocyanines as monomers/dimers with transition/pseudo metals, and double decker type phthalocyanines with some lanthanide metal ions.[7-9] The development of novel strategies for the rational design of absorption properties of Pcs using simple synthetic methods with high solubility remains a challenge in phthalocyanine chemistry. The

molecular tolerability via chemical modification and compatibility with the flexible substrates of Pcs render them ideal organic semiconductor materials as active layers for organic field effect transistors and photosensitizers in photodynamic therapy (PDT) applications.[10-12] Phthalocyanines were employed as active chemosensor materials in the development of electronic conductance, mass-sensitive, surface acoustic-wave (SAW) and optical sensors.[13-16] Several studies have investigated their sensing ability by changing both the central metal of the Pc core and the peripheral substituents for an effective detection of toxic vapours like NO_2, NH_3, SO_2, ethanol and hazardous metal ions.[17-19] The sensing mechanism was correlated with the response behaviour by formation of hydrogen bonds and the basicity of the analyte. Our recent efforts in this field have focused on the synthesis of novel porphyrins and Pcs bearing different ligands which act as molecular probes for the recognition of anions.[20] We reported a novel peripherally-substituted 2,3,9,10,16,17,23,24-octatosylamino-phthalocyanine which acts as a viable chromogenic anion chemosensor with high affinity towards fluoride ion.[21] Suitable modification of Pcs with functional ligands results in significant change of their optical properties. Liu *et al.* have developed highly selective phthalocyanine-thymine conjugates to act as selective

chemosensors for Hg^{2+}-based on target induced aggregation behaviour with fluorescence quenching.[22] Fluorogenic chemosensor based on 4-[2-(4-nitrophenoxy)ethoxy]phthalocyanine was developed for the detection of Zn^{2+} in dimethyl sulfoxide-acetonitrile medium.[23] The high planar nature of phthalocyanines promotes strong interactions (van der Waals forces, π-stacking interactions, hydrogen bonding and solvent effect) with nucleobase units, fullerene and other π-electron acceptor molecules by formation of strong charge-transfer complexes.[24] The formation of such complexes leads to dramatic changes in the Q-band spectral pattern and show quenching of the fluorescence emission behaviour.

Nitroaromatic compounds (NACs) are a class of electron-deficient compounds (known as explosive materials) who have received great attention in recent years due to homeland security threats and to their high toxicity to the environment.[25-27] Owing to their significant toxicity, ultrasensitive and selective detection of NACs is, thus, of prevalent issue. Organic thin film transistors developed with different Pcs have been employed for the detection of explosive peroxide vapours with high selectivity.[28] This study revealed that the MPc (M = metal) sensor response was primarily determined by the central metal atom, which acts as a preferential binding site while for the free phthalocyanine (H_2Pc) the inner N-H groups act as preferential hydrogen bond receptors. Teresa *et al.* developed CuPc-coated in a quartz crystal microbalance (QCM) as sensor material for oxidative combustion of nitroaromatics to $-NO_2$ in landfill gas.[29] Different MPcs and their composites with oxide networks were employed as homogeneous and heterogeneous photo-catalysts in the reduction of nitroaromatic compounds.[30] To the best of our knowledge, there are no reports on the chemosensing ability of differently substituted phthalocyanines for the detection NACs. Tuning structural modification of Pcs envisaged a greater scope for interaction with electron-deficient NAC acceptors. In this paper, we report a novel method for the synthesis of peripherally –substituted dimethylamine phthalonitriles and their corresponding Zn(II)phthalocyanines (**ZnPc1-3**) (Scheme 1). The absorption and emission properties of the newly prepared compounds were studied in both protic and aprotic solvents. The aggregation and electrochemical properties of the novel **ZnPcs** were investigated as well as the role of substituents effect on zinc (II) phthalocyanine. Covalent conjugation of dimethylamine groups with Zn(II)phthalocyanines (**ZnPc1-3**) increases their electron donating ability and makes them easier to combine with electron-acceptor nitroaromatics. Further, the interaction of **ZnPc5**, in spite of being relatively electron deficient compared to **ZnPc1-3**, was used to comprehend if there is any peripheral interaction with fluorine atoms for enhanced sensitivity and selectivity of NACs.

2. Experimental

2.1 Materials and methods

4,5-Difluorophthalonitrile, 4,5-dichlorophthalonitrile, 3,4,5,6-tetrafluorophthalonitrile, 1-chloronaphthalene, triethyl phosphite, dimethylformamide (DMF), nitroaromatic compounds such as 2,4,6-trinitrophenol (TNP), 2,4-dinitrophenol (DNP), 2,4-dinitrotoluene (DNT), 4-nitrophenol (NP), 4-nitrotoluene (NT) and nitrobenzene (NB) of analytical grade were obtained from Sigma-Aldrich and were used as received without further purification. Column chromatography was carried out on silica gel (Merck, Kieselgel 60 mesh) with the indicated eluent. All other reagents and solvents were if reagent grade and were used as received.

The NMR (^1H, ^{13}C and ^{19}F) spectra were recorded on Bruker 300 and 500 MHz NMR spectrometer and calibrated using TMS as an internal reference. Chemical shifts are reported in ppm.

Mass spectrometry studies of the final compounds were confirmed by ESI-MS MALDI-Micromass Q-TOF2 equipment.

FT-IR spectra were recorded from dry KBr pellets (infra-red spectroscopy grade, BDH SpectrosoL) using a Bruker Tensor 27 spectrometer. Typically 2 mg of the sample were mixed in a mortar with *ca.* 200 mg of KBr.

UV-Vis absorption spectra were recorded on a Shimadzu UV-2501-PC UV-Vis spectrometer. Absorption spectra in solution were recorded in $CHCl_3$ (conc. 2×10^{-6} mol/L) and the spectra in the solid state were recorded by producing thin films of **ZnPcs** on quartz substrate.

Steady-state fluorescence emission studies were carried out with Jobin-Yvon fluoroMax 3. Fluorescence quenching experiments were carried out in a quartz cell in chloroform. Stern-Volmer (SV) quenching rate constants were estimated by plotting the ratio of Io/I to the concentration of the quencher [Q], where Io and I are the maximum fluorescence intensity of the **ZnPcs** before and after the addition of the analytes, respectively. Time-resolved fluorescence measurements were carried out with time-correlated single-photon counting (TCSPC) with a picosecond LED (635 nm, pulse width <200 ps) being used to excite the samples.

Electrochemical measurements were carried out using a Metrohm Auto lab potentiostat instrument (PGSTAT-128N). Three electrode cell configurations were employed. A glassy carbon electrode having 3.0 mm in diameter was used as working electrode. A leak-free saturated Ag/AgCl electrode was employed as the reference and a Pt wire was used as the counter electrode. Tetra(n-butyl)ammonium hexa-fluorophosphate ($TBAPF_6$) was employed as the supporting electrolyte. Typically, a 0.1 M solution of $TBAPF_6$ in dimethylformamide containing 0.5 mM of **ZnPcs** was employed. The solution was purged with nitrogen flow for 3 min and voltammograms were recorded under the flow of nitrogen at ambient temperature with a scan rate of 5 mV s^{-1}.

Thin films were fabricated by taking 0.5 mg of **ZnPcs** in 0.2 mL of chloroform and spin coating on a quartz plate with a rate of 2000 rpm and annealed at 50 °C for 2 h. The fabricated thin film on the quartz plate was kept directly facing the excitation light source and the emission spectra was then collected. The position of the film was kept constant during each set of measurements. The solid state fluorescence quenching in the vapour phase was tested under saturated vapours of NACs.[27,31]

Scanning electron microscopy (SEM) images were obtained with a JEOL 7600F SEM operating at 2 kV in recorded in gentle beam mode (GB-high).

Geometry optimization of **ZnPcs** was carried out in the Gaussian 03 package with hybrid basis sets.[32] Electron density profiles of molecular orbitals were obtained with GaussView 5.0.8.

2.2 Synthesis of 4-fluoro-5-(dimethylamino)phthalonitrile, 1

4,5-Difluorophthalonitrile (492 mg, 3 mmol), dimethylformamide (DMF, 4 mL) and triethyl phosphite (100 mg) were added into a glass tube (50 mL). The glass tube was sealed tightly with a septum and heated to 160 °C for 3 h. The reaction was cool down to ambient temperature and extracted with water and chloroform (3x150 mL). The organic layer was dried over anhydrous Na_2SO_4 and the solution was evaporated under reduced pressure. The crude product was purified by column chromatography over silica gel (dichloromethane: hexane, 1:1) and recrystallized from $CHCl_3$ and MeOH gave pale yellow solid **1** with *ca.* 72% yield. ^1H NMR (300 MHz, $CDCl_3$): δ 7.31 (d, 1H, J =12 Hz), 7.0 (d, 1H, J = 6 Hz), 3.08 (s, 6H). ^{19}F NMR (282.38 MHz, $CDCl_3$): δ 137.67 (t, J = 19.7 Hz, 1F). ^{13}C NMR (75.47 MHz, $CDCl_3$): δ 42.0 (-N(CH_3)$_2$), 107.2, 115.6, 121.1, 143.5, 147.4, 154.9. ESI-MS: m/z calculated for $C_{10}H_8FN_3$: 189.07; found: 190.1 $[M+H]^+$. FT-IR (KBr pellet), v_{max}/cm^{-1}: ν(C-H) = 2908-2883 w; ν(C≡N) = 2220 s ; ν(C=C) = 1584, 1512 s; β(C-H) =

1469 vs; ν(C-H) = 1424 vs; ν(C-C) = 1389 s; ν(C-N) = 1239 m; ν(C-N) = 1020 m; γ(C-H) = 965 s, 737 w.

Synthesis of 4-chloro-5-(dimethylamino)phthalonitrile, 2

4,5-Dichlorophthalonitrile (586 mg, 3 mmol), dimethyl-formamide (DMF, 4 mL) and triethyl phosphite (100 mg) were added into a glass tube (50 mL). The glass tube was sealed tightly with a septum and heated to 160 °C for 6 h. After completion of the reaction, the tube was cool down to ambient temperature and the mixture was washed with water and extracted with chloroform (3x50 mL). The organic layer was dried over anhydrous Na_2SO_4. The solvent was evaporated under reduced pressure and the crude product was purified by column chromatography over silica gel (dichloromethane: hexane, 3:2) and recrystallized from chloroform and methanol producing the yellow solid **2** with a yield of *ca.* 76% (467 mg). ^{1}H NMR (300 MHz, $CDCl_3$): δ 7.68 (s, 1H), 7.20 (s, 1H), 3.02 (s, 6H, CH_3). ^{13}C NMR (75.47 MHz, $CDCl_3$): δ 42.8 (-N(CH_3)$_2$), 106.2, 115.1, 122.9, 129.6, 135.8, 153.7. ESI-MS: m/z calculated for $C_{10}H_8ClN_3$: 205.1; found, 206.1 [M+H]$^+$. FT-IR (KBr pellet), $ν_{max}/cm^{-1}$: ν(O-H, water) = 3113 m ; ν(C-H) = 2911-2856 w; ν(C≡N) = 2220 m ; ν(C=C) = 1584, 1522 s; ν(C-H) = 1428 vs; ν(C-C) = 1389 s; ν(C-N) = 1274 w; ν(C-N) = 1009 m; γ(C-H) = 894 s, 735 w.

Synthesis of 4,5-bis(dimethylamino)-3,6-difluorophthalonitrile, 3

3,4,5,6-Tetrafluorophthalonitrile (600 mg, 3 mmol), dimethyl-formamide (DMF, 4 mL) and triethyl phosphite (100 mg) were added into a glass tube (50 mL). The tube was sealed tightly with a septum and heated to 160 °C for 6 h. The reaction mixture was cool down to ambient temperature and washed with water and extracted with chloroform (3x50 mL), being observed the formation of two different products during the reaction. The organic layer was dried over anhydrous Na_2SO_4 and the solvent was evaporated under reduced pressure. The crude product was purified by column chromatography over silica gel using a mixture of dichloromethane:hexane (3:2) as eluent. The major yellow compound was identified as compound **3** in 68% yield. The other compound, with a yield of 22%, was identified as 4-(dimethylamino)-3,6-difluorophthalonitrile (**4**).

Compound **3**: ^{1}H NMR (300 MHz, $CDCl_3$): δ 3.13 (s, 12H, CH_3). ^{19}F NMR (282.38 MHz, $CDCl_3$): δ 129.70 (t, *J* = 22.6 Hz, 2F). ^{13}C NMR (75.47 MHz, $CDCl_3$): δ 41.7 (-N(CH_3)$_2$), 95.6, 111.2, 140.2, 154. 4. ESI-MS: m/z calcd for $C_{12}H_{12}F_2N_4$, 250.1; found; 251.1 [M+H]$^+$. FT-IR (KBr pellet), $ν_{max}/cm^{-1}$: ν(O-H, water) = 3310 m ; ν(C-H) = 3051-2839 w; ν(C≡N) = 2220 m; ν(C=C) = 1584 s; ν(C-H) = 1442 vs; ν(C-C) = 1371 m; ν(C-N) = 1248 m; β(C-H) = 1117 w; ν(C-N) = 1062 m; γ(C-H) = 930 s, 735 w.

Compound **4**: ^{1}H NMR (300 MHz, $CDCl_3$): δ 7.33 (s, 1H), 3.11 (s, 6H, CH_3). ^{19}F NMR (282.38 MHz, $CDCl_3$): δ 137.68 (t, *J* = 19.7 Hz, 1F), 145.1(t, *J* = 16.9 Hz, 1F). ^{13}C NMR (75.47 MHz, $CDCl_3$): δ 42.6 (-N(CH_3)$_2$), 106.5, 115.4, 123.2, 129.3, 136.1, 153.3. ESI-MS: m/z calculated for $C_{10}H_8ClN_3$: 207.1; found, 208.1 [M+H]$^+$

Synthesis of tetrakis[4-fluoro-5-(dimethylamino) phthalocyaninato]cinc(II), ZnPc1

Zinc dust (0.327 g), 4-fluoro-5-(dimethylamino)phthalonitrile, **1** (0.472 g, 2.5 mmol) and 1-chloronapthalene (10 mL) were stirred and heated under reflux at 200 °C for 48 h in a sand bath. The reaction mixture was cool down to ambient temperature after which petroleum ether was added. The formed precipitate was filtered and the resulting residue was stirred with 2M hydrochloric acid (50 mL) in order to dissolve the unreated zinc. The residual dark green solid was washed with boiling water, dried, finely powdered and extracted

with chloroform (2x100 mL). The solution was evaporated under reduced pressure and purified through silica gel column chromatography with a chloroform:methanol mixture (98:2) to isolate **ZnPc1** in 66% yield. ^{1}H NMR (300 MHz, $CDCl_3$+triethylamine): δ 9.15 (d, *J* = 12 Hz, 2H, α-Pc), 9.06 (d, *J* = 18 Hz, 2H, α-Pc), 8.87 (d, *J* = 9Hz, 2H, α-Pc), 8.82 (d, *J* = 3 Hz, 2H, α-Pc), 3.37(s, -N(CH_3)$_2$, 24H). ^{19}F NMR (282.38 MHz): δ 142.12 (t, *J* = 28.2 Hz, β-F). ^{13}C NMR (125.77 MHz, DMSO-d_6): δ 43.9 (t, *J* = 16.3 Hz, (-N(CH_3)$_2$), 112.3 (d, *J* = 32.7), 123.7-123.4 (q), 128.3 (t, *J* = 15.1 Hz), 131.7 (t, *J* = 40.2 Hz), 137.2-136.3 (m), 151.2-149.6 (m). MALDI-TOF MS: m/z calculated for $C_{40}H_{32}F_4N_{12}Zn$, 820.2; found; 820.2 [M]$^+$. FT-IR (KBr pellet), $ν_{max}/cm^{-1}$: ν(O-H, water) = 3432 m ; ν(C-H) = 2926-2804 w; ν(C=C) = 1627 w; ν(C-H) = 1418 vs; ν(C-C)$_{isoindole}$ = 1321 m; ν(C-N) = 1286 m; β(C-H) = 1112 s; ν(C-N)$_{pyrrole}$ = 1043 m; γ(C-H) = 973 s, 737 w.

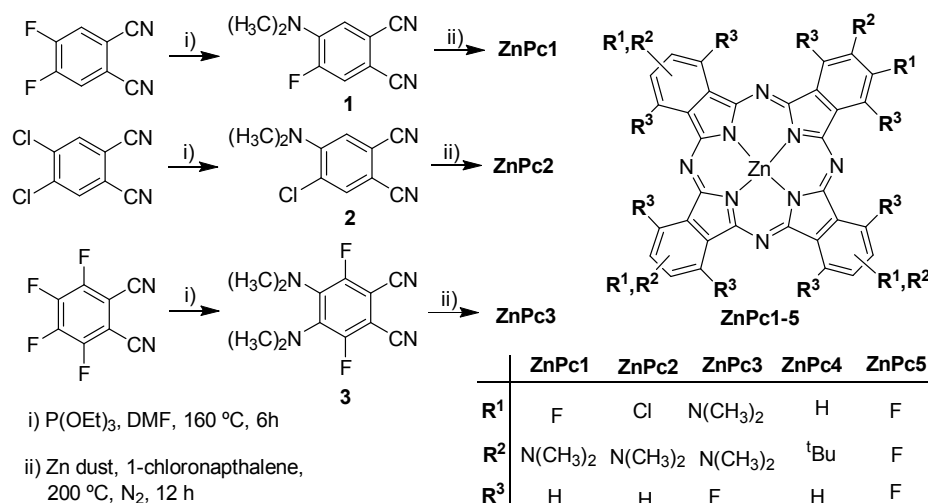**Synthesis of tetrakis[4-chloro-5-(dimethylamino) phthalocyaninato]zinc(II), ZnPc2**

A similar procedure as described for **ZnPc1** was employed for the preparation of **ZnPc2** using 4-chloro-5-(dimethylamino) phthalonitrile **2** as precursor. Yield: 62%. ^{1}H NMR (300 MHz, DMSO-d_6): δ 8.81-8.72 (m, 2H, α-Pc), 8.67-8.55 (m, 4H, α-Pc), 8.40 (d, *J* = 12Hz, 2H, α-Pc), 3.46 (s, 24H, -N(CH_3)$_2$). ^{13}C NMR (125.77 MHz, DMSO-d_6): δ 43.9 (t, *J* = 15.1 Hz, (-N(CH_3)$_2$), 112.2 (d, *J* = 23.9), 123.7-123.4 (q), 128.6 (t, *J* = 27.6 Hz), 131.7 (t, *J* = 40.2 Hz), 137.1-136.5 (m), 151.3-149.7 (m). MALDI-TOF MS: m/z calculated for $C_{40}H_{32}Cl_4N_{12}Zn$, 884.1; found 886.1 [M+H]$^+$. FT-IR (KBr pellet), $ν_{max}/cm^{-1}$: ν(O-H, water) = 3397 m ; ν(C-H) = 2935-2778 w; ν(C=C) = 1609 w; ν(C-H) = 1409 vs; ν(C-C)$_{isoindole}$ = 1321 w; ν(C-N) = 1286 w; β(C-H) = 1103 s; ν(C-N)$_{pyrrole}$ = 1068 m; γ(C-H) = 990 s, 746 w.

Synthesis of octakis[4,5-bis(dimethylamino)-3,6-difluorophthalocyaninato]zinc(II), ZnPc3

A similar procedure as described for **ZnPc1** was employed for the preparation of **ZnPc3**, using 4,5-bis(dimethylamino)-3,6-difluorophthalonitrile **3** as precursor. Yield: 68%. ^{1}H NMR (300 MHz, DMSO-d_6): 3.43 (s, 24H, -N(CH_3)$_2$). ^{19}F NMR (282.38 MHz, DMSO-d_6): δ 131.45 (t, *J* = 14.1 Hz, 8F). ^{13}C NMR (125.77 MHz, DMSO-d_6): δ 43.9 (t, *J* = 15.1 Hz, (-N(CH_3)$_2$), 112.7, 128.8, 133.2, 137.5, 151.5. MALDI-TOF MS: m/z calculated for $C_{48}H_{48}F_8N_{16}Zn$, 1064.3; found 1066.3, [M+H]$^+$. FT-IR (KBr pellet), $ν_{max}/cm^{-1}$: ν(O-H, water) = 3310 m ; ν(C-H) = 2952-2795 w; ν(C=C) = 1609 s; ν(C-H) = 1400 vs; ν(C-C)$_{isoindole}$ = 1339 m; ν(C-N) = 1243 m; β(C-H) = 1138 w; ν(C-N)$_{pyrrole}$ = 1025 m; γ(C-H) = 946 s, 737 w.

3. Results and discussion

The synthetic route employed for the preparation of new peripheral dimethylamine substituted ZnPcs is depicted in Scheme 1. An interesting finding was noted while optimizing the reaction conditions for the nucleophilic substitution of phthalonitriles with triethyl phosphite. The treatment of 4,5-difluorophthalonitrile with triethyl phosphite in DMF at 160 °C leads to formation of 4-fluoro-5-(dimethylamino)phthalonitrile (**1**) in good yield. Reaction of 3,4,5,6-tetrafluorophthalonitrile forms 4,5-bis(dimethylamino)-3,6-difluorophthalonitrile (**3**) as major product (yield 68%) along with the formation of 4-(dimethylamino)-3,6-difluorophthalonitrile as a secondary product (**4**) with yield of 22%. The formation of dimethylamine substitution on phthalonitriles could involve the reaction of substrate with DMF followed by the loss of carbon monoxide or nucleophilic substitution of dimethylamine formed by the decomposition of DMF. We have discovered that

i) P(OEt)$_3$, DMF, 160 °C, 6h

ii) Zn dust, 1-chloronapthalene, 200 °C, N$_2$, 12 h

	ZnPc1	ZnPc2	ZnPc3	ZnPc4	ZnPc5
R^1	F	Cl	N(CH$_3$)$_2$	H	F
R^2	N(CH$_3$)$_2$	N(CH$_3$)$_2$	N(CH$_3$)$_2$	^{t}Bu	F
R^3	H	H	F	H	F

Scheme 1. Synthesis of dimethylamine-substituted phthalonitriles and their zinc(II)-based phthalocyanine.
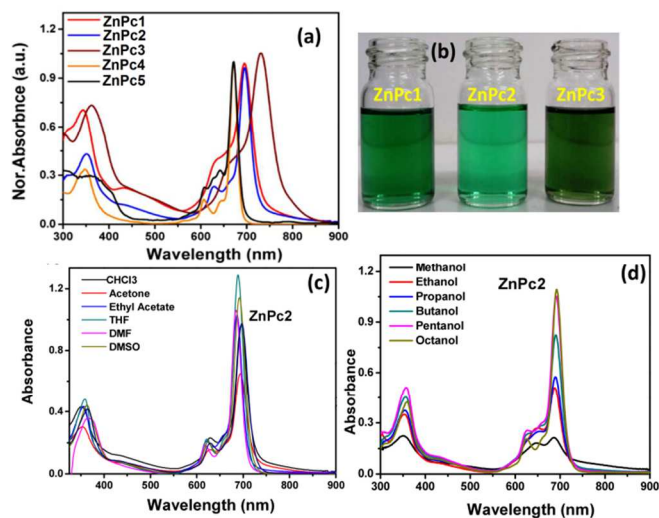

Fig. 1 Crystallographic determination of the crystal structures of the dimethylamine substituted phthalonitriles **1** to **3**. Non-hydrogen atoms are represented as thermal ellipsoids drawn at the 50% probability level and hydrogen atoms as small spheres with arbitrary radii.

triehtyl phosphite acts as a catalyst for the fast decomposition of DMF ultimately promoting the nucleophilic substitution of the dimethylamine groups on the phthalonitrile. Under similar experimental conditions, in the absence triethyl phosphite and the use of other bases such as Na$_2$CO$_3$, K$_2$CO$_3$ and Cs$_2$CO$_3$, the formation of the corresponding dimethylamine-substituted phthalonitrile derivatives are typically observed with very low yields in the range of 10-26% for a total reaction time of 24 h. Table S1 summarizes the experimental reaction conditions and use of different amounts of triethyl phosphite, and other bases, for the formation of dimethylamine phthalonitriles from the corresponding phthalonitriles. Increasing the amount of triethyl phosphite in the reaction medium promotes a great enhancement of the product conversion rate. We note that the dimethylamination of aromatic compounds with DMF has been reported to be dependent on the employed temperature.[33] At elevated temperatures, fluoro/chloro groups undergo nucleophilic substitution that depends on the activation of the fluoro/chloro groups induced by the cyano group of phthalonitriles. As the fluoro/chloro groups exert its strong electron withdrawing effect, dimethylamination occurs only at the β-position while halogens at α-positions are unaffected. In short, the results herein presented clearly demonstrate that a combination of DMF and triethyl phosphite could serve as a better and more efficient approach to produce selective dimethylamine phthalonitriles when treated with halogenated phthalonitriles. The NMR (^{1}H, ^{19}F and ^{13}C), ESI-MS spectra (Figs. S1-S11, ESI†) and single-crystal X-ray diffraction studies corroborate in tandem the structural features of the prepared dimethylamine-substituted phthalonitriles. Good quality single-crystals suitable X-ray diffraction studies were obtained by slow

solvent evaporation of a solution of each pure compound in a chloroform-methanol (1:1) mixture at ambient temperature. Fig. 1 depicts the molecular structures as derived from these studies for **1** to **3**. Zinc(II) phthalocyanines (ZnPcs) were prepared via a cyclotetramerization reaction of the respective phthalonitriles and metallic zinc in 1-chloronaphthalene at 200 °C. The cyclotetramerization of the dimethylamine-substituted precursors **1** and **2** in the presence of anhydrous ZnCl$_2$ in 1-chloronaphthalene inevitably led to the formation of **ZnPc1** and **ZnPc2** as mixtures of four regioisomers having C_{4h}, C_{2v}, C_s and D_{2h} point symmetry symmetry. The structures of the target compounds were confirmed from FT-IR (Figs. S12-13, ESI†), NMR (^{1}H, ^{13}C and ^{19}F) and MALDI-TOF-mass spectroscopic techniques (Figs. S14-S24, ESI†). The FT-IR spectra of **ZnPc1-3** exhibit major bands arising from the central aromatic Pc macrocycle including the wagging and torsion vibrations of C-H groups *ca.* 2943−2795 cm^{-1}, C=C modes in the range *ca.*1609-1627 cm^{-1}, and C−C isoindole ring stretching vibrations in the range *ca.* 1321-1389 cm^{-1}. In addition, the absence of C≡N peaks at *ca.* 2220 cm^{-1} in the spectra clearly indicated that the precursor phthalonitriles 1–3 were converted into **ZnPc1-3**. The ^{1}H NMR spectra of **ZnPc1** show four doublet peaks in the range δ 9.15-8.82 ppm arising from the resonances of the α-protons corresponding to the four isomers; the dimethylamine (−N(CH$_3$)$_2$) protons appear as a singlet peak at δ 3.37 ppm. ^{19}F NMR shows a triplet with J = 28.3 Hz. ZnPc3 shows only −N(CH$_3$)$_2$ protons at δ 3.43 ppm, while the ^{19}F NMR is dominated by a triplet peak centred at δ 131.45 with J = 14.1 Hz corresponds to the α-F atoms. The mass spectra of all ZnPcs exhibit an intense cluster corresponding to aggregates of molecular ion peaks centred at m/z 820.2 for **ZnPc1**,
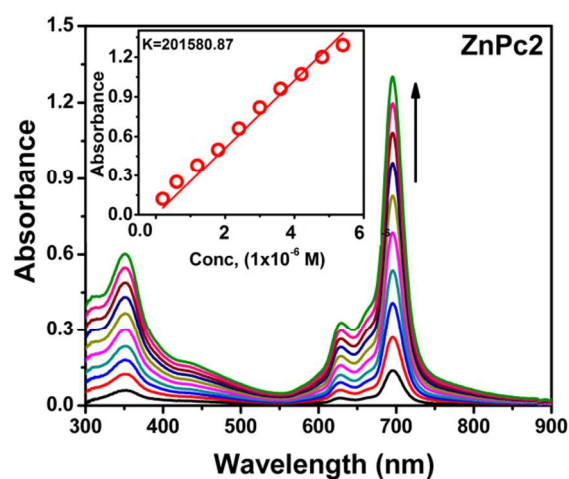
[M+H]$^+$ at 886.1 for **ZnPc2** and [M+H]$^+$ at 1066.3 for **ZnPc3** respectively (Figs. S16-18, ESI†). The UV-Vis spectra (Fig. 2) of **ZnPc1–3** exhibit an intense Q-band absorption in the region of 650-730 nm and another at 600−650 nm. These bands are attributed to the π→π* transitions from the highest occupied molecular orbital (HOMO) to the lowest unoccupied molecular orbital (LUMO) of the Pc ring. The position of Q-band varied with the nature and number of the pendant dimethylamine groups on phthalocyanine core. **ZnPc3** exhibits *ca.* 19 nm and 27 nm red shifts in comparison with **ZnPc1** and **ZnPc2**. This illustrates well that the high electron-donating ability of dimethylamino groups leads to a larger destabilization of the HOMO orbitals and results in a decrease of the HOMO–LUMO gap. The broad band in the range of 440–530 nm is probably due to charge transfer from the electron-rich ring to the electron-poor metal centre. The other B bands in the UV region located at *ca.* 305–390 nm are due to transitions from the deeper π levels to the LUMO. The dimethylamine derived **ZnPc1-3** molecules are soluble in various solvents such as tetrahydrofuran (THF), acetone, dichloromethane (DCM), chloroform (CHCl$_3$), dimethyl-sulfoxide (DMSO) and DMF, with this properties being attributed to the presence of the dimethylamine (–N(CH$_3$)$_2$) groups in the periphery of the macrocycle. Fig. 2b depicts the variation in colour of **ZnPc1-3** in CHCl$_3$.

coefficient (ε). The ε values were determined and summarized in Table S1. An interesting feature was observed in the Q-band of **ZnPc1-3** in protic solvents. In methanol solution, the intensity of the Q-band decreases dramatically and shows a broad absorption with an overlap of the peak at 630 nm. Such spectral features are typical for Pc dimers or aggregates.[34] The intensity of the Q-band increases as the length of alkyl chain of the protic solvents is also increased (*i.e.*, from methanol to octanol). Fig. 2d shows the change in the absorption spectral pattern of **ZnPc2** in different protic solvents. The absorption of Q-band shows a red shift of 8-10 nm with a dramatic increase in the absorption co-efficient value in respect to the increase of the alkyl chain of alcoholic solvents. According to Kasha's exciton theory, Zn(II)phthalocyanines (**ZnPc1-3**) form H-type aggregates by the occurrence of strong intermolecular π–π stacking interactions.[35] These aggregates were, however, dissociated into monomers having an enhanced Q-band intensity with the increase in the alkyl chain length of the solvent, going from methanol to octanol. The absorption spectra of other **ZnPcs** in different solvents are depicted in Fig. S25 (ESI†). The aggregation behaviour of **ZnPc1-3** was studied by collecting the concentration-dependent UV-Vis spectra in chloroform (Fig. S26, ESI†). Fig. 3 shows the representative concentration dependent absorption spectra of **ZnPc2** in chloroform.

Fig. 2 (a) Absorption spectra of **ZnPc1-5** in chloroform. **(b)** Photograph showing the variation in colour of different **ZnPcs** in chloroform. **(c)** Absorption spectra of **ZnPc2** in different solvents and **(d)** in different alcohol solvents.

The UV-Vis spectra of 2.0×10^{-6} M of **ZnPc1-3** in various solvents (aprotic) exhibited sharp and non-split Q-bands absorption bands, which are characteristic of monomeric forms for **ZnPc1-3**. We note that the employed solvents of each investigated class were chosen so to cover a wide permittivity range. The position of the Q-band varies with the refractive indices of the solvents: the higher refractive index of the solvent, the more red-shifted the Q-band. **ZnPc1-3** show Q-band peaks at 691, 682 and 704 nm in THF with a refractive index of 1.406, and at 700, 695 and 722 nm, respectively, in DMSO with a refractive index of 1.479. Thus, the replacement of a solvent with a higher refractive index results in a red shift of the Q-band in the range of 5-15 nm (Fig. 2c). The absorption co-efficient of **ZnPc1-3** have a strong influence on the solvent polarities. In addition to the position of the absorption, the intensity of the Q-band was quantified by the molar extinction


Fig. 3 Variation of the absorption spectra of **ZnPc2** in chloroform with respect to the concentration of the solution. The inset shows the change in the absorbance of the Q-band at 698 nm for different concentrations of **ZnPc2**.

The intensity of Q-band increases gradually with the increase of the concentration without any appearance of new absorption bands. This process followed the Beer-Lambert law, which is characteristic of non-aggregated Pcs, in the concentration range from 2x10^{-7} to 3x10^{-6} mol dm^{-3}. The inset in Fig. 3 shows the linear increase in the absorbance as a function of the concentration. Steady-state fluorescence emission studies provide information on the fluorescence excitation and emission wavelengths, Stokes shift and the fluorescence quantum yields. Fig. 4a shows the emission spectra of **ZnPcs** in chloroform under excitation at 630 nm. **ZnPc3** shows a red shifted emission spectra with an emission shift of *ca.* 20 nm and 24 nm in comparison with **ZnPc1** and **ZnPc2**, respectively. It was found that while increasing the number of dimethylamine groups on **ZnPcs**, the emission spectral pattern is more red shifted comparing to the absorption spectra. In DMSO, **ZnPc1-3** exhibits a red shifted emission when compared with other

solvents. The emission spectra of all complexes show emission bands that are typical for phthalocyanines with Stokes shift ranging from 5-20 nm. The fluorescence emission spectra of **ZnPc1-3** were performed in different solvents. The emission maximum was found to vary according to the solvent polarity. In methanol, **ZnPcs** exhibit very low fluorescence emission intensity. This arises because of the formation of aggregates as clearly observed in the absorption spectra.
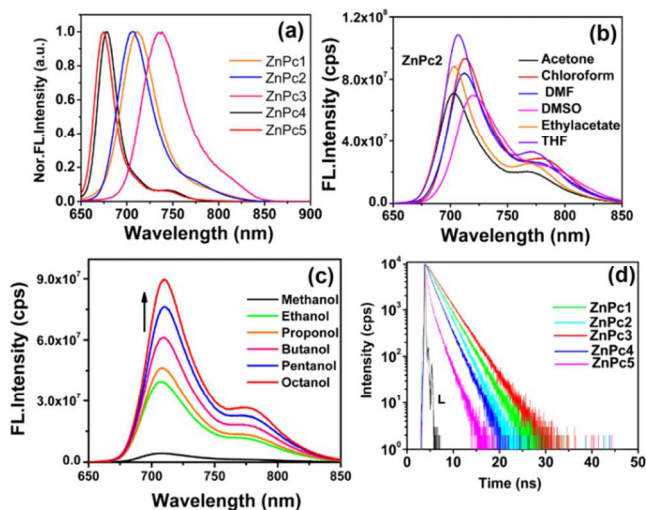
Fig. 4 (a) Steady-state fluorescence emission spectra of **ZnPc1-5** in chloroform upon excitation at λ_{ex} = 630 nm. (b) Emission spectra of **ZnPc2** in different solvents. (c) Change in the emission behaviour of **ZnPc2** in different alcoholic solvents on excitation at λ_{ex} = 630 nm. (d) Time-resolved fluorescence emission decay of **ZnPc1-5** in chloroform. The decay "L" represents the instrument response function.

Aggregates of Pcs are known to quench the fluorescence emission because aggregation lowers the fluorescence intensity of molecules through dissipation of energy.[36] The emission intensity increases with increasing the alkyl chain of the alcohol medium (Fig. S27, ESI[†]). A study of the dependence of the emission with the concentration reveals that the emission maximum is red shifted. For example, the emission maxima of **ZnPc3** show a gradual red shift as a function of the concentration $(1 \times 10^{-6} - 6 \times 10^{-6}$ M) and starts decreasing in

intensity without any change in the spectral pattern (Fig. S28, ESI[†]). This indicates the formation of molecular aggregates of **ZnPcs** at this concentration level. The fluorescence quantum yields of **ZnPc1-3**, in different solvents were measured using **ZnPc** as the reference.[1,2a] The compounds exhibit fluorescence quantum yields in the range 0.02-0.15 in different solvents. We note that the very low quantum yields were observed for **ZnPc1-3** in methanol. The fluorescence lifetime with time-correlated single photon counting (TCSPC) method was measured for **ZnPc1-3**, with the values showing single exponential emission decays with lifetimes of *ca.* 1.85 ns, 2.81 ns and 3.22 ns for **ZnPc1**, **ZnPc2** and **ZnPc3**, respectively. **ZnPc3** exhibits longer lifetime than **ZnPc1** and **ZnPc2** because of its more symmetrical nature and increased donating strength. The fluorescence rate constants ($k_f = \Phi_F/\tau_F$) and non-radiative rate constants ($k_{nr} = (1-\Phi_F)/\tau_F$) were calculated and the photophysical data of **ZnPc1-5** in chloroform are summarized in Table 1. Data for other solvents are summarized in Tables S2 and S3 (ESI[†]).

The electrochemical properties of the **ZnPc1-3** were investigated using cyclic voltammetry (CV) in dimethyl-formamide containing 0.1 M tetrabutylammonium hexafluorophosphate (TBAPF$_6$) with Ag/AgCl as the reference electrode. Because the central zinc cation is redox inactive, all the observed processes are attributed to successive removal/addition of electrons from/to the ligand-based orbitals. Fig. 5 shows the cyclic voltammogram of **ZnPc1-3** with a scan rate of 0.05 V s^{-1}. **ZnPc1-3** exhibit one quasi-reversible and one reversible reduction peak with the first reduction potential ($E_{1/2}$) appearing at -0.35 ± 0.02 V, and a second reduction potential ($E_{1/2}$) at 1.08 ± 0.03V in the cathodic region. These values are in agreement with previous reports showing alkyl dimethylamine substituted **ZnPcs** undergoing similar redox processes.[37] The reduction potential of **ZnPc3** was slightly less than **ZnPc1** and **ZnPc2** indicating that the LUMO energy level was affected by substitution. For all molecules, one electron exchange was involved in the second reduction region. The peak currents of the processes exhibited a linear increase with the square root of the scan rates ranging from 20 to 100 mV s^{-1}, indicating that the electrode reactions are diffusion-controlled through the solvent medium. The photophysical and electrochemical properties of **ZnPc4** and **ZnPc5** was found to be similar and the properties of these compounds are well documented in the literature.[1,2a]

Table 1. Summary of photophysical data of **ZnPc1-3** in chloroform.

Compd.	Abs, nm (log ε)[a]	Emission nm[b]	Stokes shift (nm)	Q.Y.[c] (Φ_F)	Lifetime τ_f (ns)	K_f (s^{-1}) (10^6)[d]	K_{nr} (s^{-1}) (10^6)[e]
ZnPc1	359 (4.44), 636 (4.11), 701 (5.49)	717, 783	16	0.12	1.85	64.86	475.67
ZnPc2	347 (5.16), 621 (4.83) 693 (5.50)	713, 784	20	0.10	2.81	35.58	320.28
ZnPc3	358 (5.06), 646 (4.65) 720 (5.27)	737, 813	17	0.16	3.22	49.68	260.86

[a] log ε represents the molar absorption coefficients; [b] Excitation at λ_{ex}: 630 nm; [c] reference to ZnPc (Φ_F) = 0.20; [d] $K_f = \Phi_F/\tau_F$; [e] $K_{nr} = 1- \Phi_F/\tau_F$.
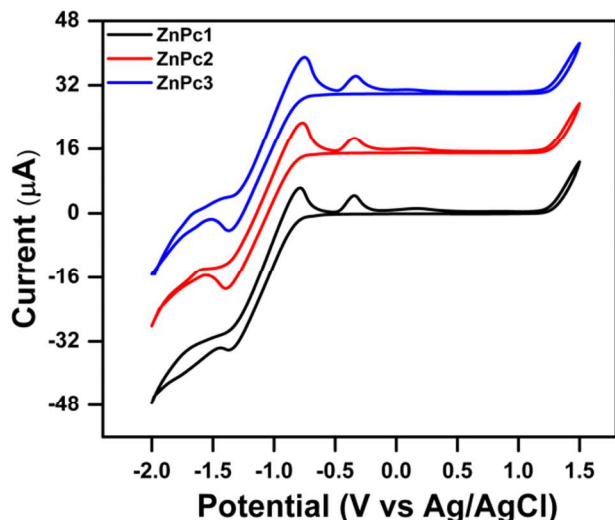
Fig. 5 Cyclic voltammogram of **ZnPc1-3** in dimethylformamide.

A number of reports have appeared in the literature describing the ability of **ZnPcs** in electron transfer processes with acceptors.[24] The formation of donor-acceptor charge transfer complexes could involve π-π stacking and intra/inter molecular interactions. Nitroaromatic compounds (NACs) are known to behave as good acceptors, and detection of NACs has recently attracted increased attention.[37-39] We further tested the usage of **ZnPc1-3** towards the detection of NACs through fluorescence quenching in solution and in the solid state. To demonstrate the ability of **ZnPc1-3** for detection of NACs we first performed fluorescence quenching studies of **ZnPc1-3** with different NACs such as 4-nitrobenzene (NB), 4-nitrotoluene (NT), 4-nitrophenol (NP), 2,4-dinitrotoluene (DNT), 2,4-dinitrophenol (DNP), 2,4,6-trinitrophenol (TNP), 2,4,6-trinitrotoluene (TNT), nitromethane (NM) and other aromatic electron-deficient compounds such as benzoquinone (BQ) and 2,3-dichloro-5,6-dicyano-1,4-benzoquinone (DDQ) in chloroform. According to the undertaken study, **ZnPcs** exhibit good fluorescence quenching behaviour towards trinitrophenol (TNP). To corroborate the selectivity of **ZnPcs** for the detection of NACs, we have carried out fluorescence titration experiments with other electron-deficient aromatic compounds. Interestingly, **ZnPcs** showed differential fluorescence quenching responses among the various tested analytes. Fig. 6a shows the emission spectra of **ZnPc3** upon the gradual addition of different concentrations of TNP under excitation at 630 nm. The emission maxima of **ZnPc3** at 737 nm depleted with the increased concentration of TNP in solution, showing 80% quenching at 450 μM of TNP concentration (~103±2 ppm). **ZnPc1** and **ZnPc2** show 41% and 58% of quenching efficiency for TNP, respectively. These results indicate that the increase in the number of dimethylamine groups on the ZnPc enhances the electron donating strength of the macrocycle ultimately showing a high quenching efficiency. To further understand this phenomenon, we have studied two model compounds consisting of *t*-butyl substituted groups at peripheral positions of **ZnPc** as more electron donating (**ZnPc4**) and
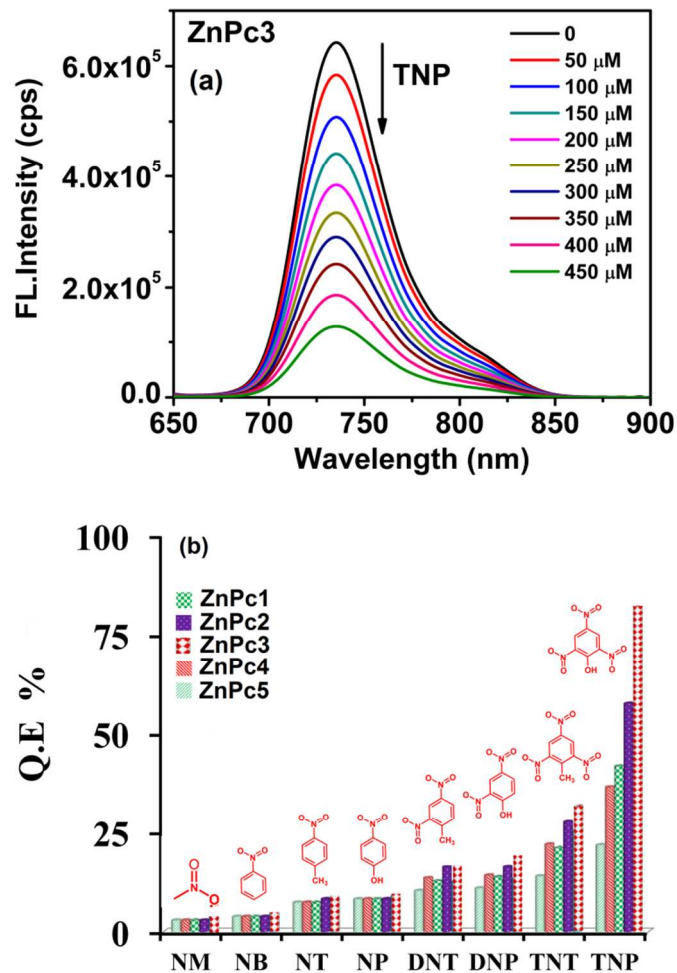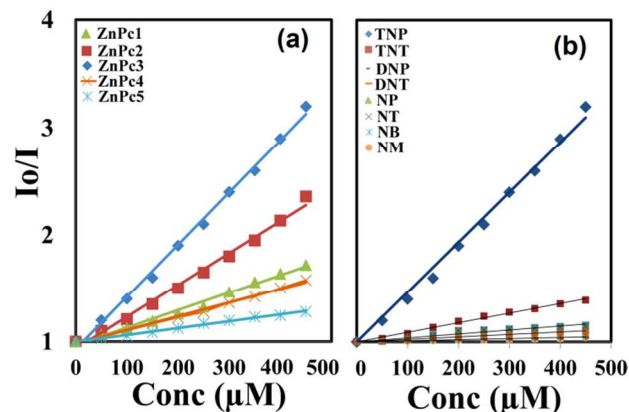

Fig. 6 (a) Fluorescence quenching behaviour of **ZnPc3** upon addition of different concentrations of TNP in chloroform. (b) Comparative quenching efficiency of **ZnPc1-5** treated with different NACs.

highly electron withdrawing perfluoro substituted groups (**ZnPc5**) (see Scheme 1) with NACs. Under similar experimental conditions, **ZnPc4** and **ZnPc5** show only 36% and 21% of quenching efficiency for TNP. The high electron donating strength of dimethylamine groups in **ZnPc1-3** show higher sensitivity than **ZnPc4**. The less quenching efficiency **ZnPc5** arises due to the high electron withdrawing tendency of fluorine making **ZnPc5** a more electro-deficient compound than other **ZnPcs** used in this work, and also exhibiting weak interactions with NACs (Figs. S29-33, ESI[†]). These results are consistent with the observations for other fluoro-derivatives of porphyrins treated with different nitrated derivatives.[41] Fig. 6b depict the quenching efficiency of **ZnPcs** when treated with different NACs. Results show that **ZnPcs** exhibit high selectivity towards trinitrophenol with **ZnPc3** showing a superior selectivity than other **ZnPc** derivatives. Quantitative evaluation of the solution phase quenching of fluorescence was performed using the Stern–Volmer (SV) equation, where Io and I are the fluorescence intensities in the absence and in the presence of the analyte, respectively, Q is the analyte concentration and K_{SV} is the Stern–Volmer rate constant. The steady-state Stern–Volmer plots provide more insight so to understand the quenching mechanism is static or dynamic. The static quenching was formed by ground state complex

between ZnPcs and NACs and dynamic quenching was formed by excited state collisions.


Fig. 7 (a) The Stren-Volmer (SV) plot of **ZnPc1-5** treated with different concentrations of TNP. (b) The SV plot of **ZnPc3** upon addition of different NACs at different concentration levels.

Fig. 7a shows the SV plot of **ZnPcs** treated with different concentrations of TNP. All **ZnPcs** exhibit a linear increase in the Io/I values with respect to the degree of fluorescence quenching, indicating a static quenching by formation of ground state complexes between **ZnPcs** and TNP. Among all **ZnPcs** studied, **ZnPc3** shows the higher quenching rate constant of $2.99 \times 10^4\,M^{-1}$ with the order of reactivity being **ZnPc3>ZnPc2>ZnPc1>ZnPc4>ZnPc5** for TNP. The significant high magnitude of K_{sv} for **ZnPc3** when compared to **ZnPc1** and **ZnPc2** is attributed to the additional supra-molecular interactions. Fig. 7b shows the SV plot **ZnPc3** for different NACs. Table S4 (ESI[†]) summarizes the SV rate constants of **ZnPcs** with different NACs. The formation of static quenching was further confirmed by UV-Visible titration of **ZnPcs** with TNP. For instance, when adding different concentrations of TNP to **ZnPc3**, the intensity of the Q-band peak at *ca.* 720 nm decreases as a function of the concentration, while the intensity of the peak at *ca.* 640 nm gradually increases. The high selectivity towards TNP arises due to its absorption at *ca.* 340 nm, which overlaps with the absorption spectra of the soret band of ZnPcs. The intensity of the Soret increases with the increase of the concentration of TNP (Fig. S35, ESI[†]) indicating the formation of charge-transfer complexes by axial coordination of the TNP molecules to **ZnPcs**, in a similar fashion to the reported axial coordination of Zn(II)porphyrins with NACs alongside with the formation of strong intermolecular π-π stacking interactions by co-facial geometry.[42] On the other hand, ZnPcs exhibit moderate quenching of the fluorescence by other electron-deficient compounds (benzoquinone, DDQ and aromatic solvents such as benzene and toluene) and their quenching efficiency is quite low in magnitude when compared to all nitroaromatics. The stoichiometric binding constants of ZnPcs treated with different concentrations of TNP were determined by using the Benesi–Hildebrand equation.[43] The observed linear fits with TNP indicate formation of 1:1 adducts and **ZnPc3** show high binding affinity (Fig. S34, ESI[†]).

Based on the collected photophysical studies, we observe that there is no spectral overlap between the absorption spectrum of TNP and the emission spectra of **ZnPcs**, thus indicating that the main quenching mechanism is due to photo-induced charge transfer between the excited states of the **ZnPcs** to NACs. Furthermore, so a favourable electron to be transferred from the excited state of sensor

to the analyte leads to observed fluorescence quenching. This can be understood better one needs to take a close look at the energy levels of **ZnPcs** and NACs. Density Functional Theory (DFT) calculations were carried out using Gaussian03 with basis set as B3LYP/6-31g* with LANL2DZ. Tetra-substituted **ZnPcs** were isolated as different regioisomers with C_{4h}, D_{2h}, C_{2v} and C_s symmetries. Spectroscopic data show, however, 50% probability of obtaining the C_{4h} symmetry as stable conformer with high yield.[4] Therefore, all **ZnPcs** were optimized with point C_{4h} symmetry for better correlation of **ZnPc1**, **ZnPc2** and **ZnPc3**. The optimized structures are in good agreement with similar structures obtained from experimental studies.[44] Frequency calculations were carried out for the optimized structures in order to confirm that all structures considered are minima on the potential energy surface.
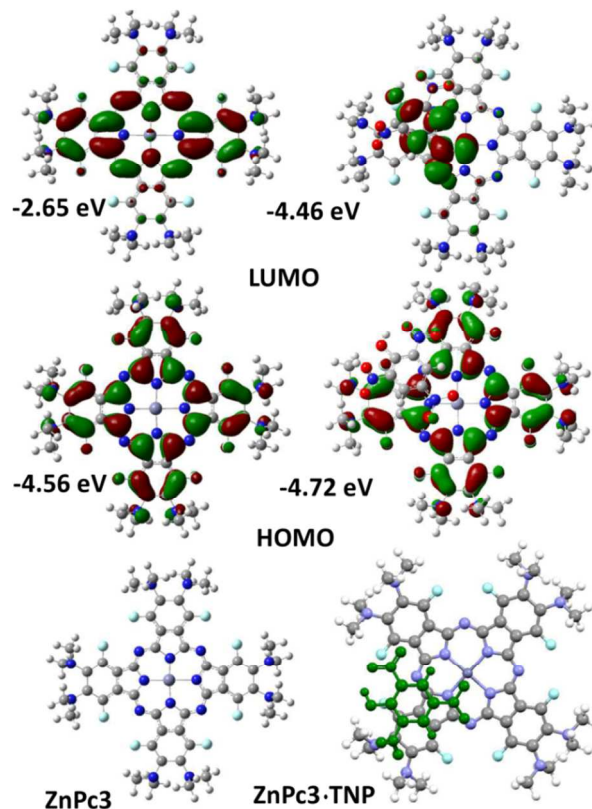
Fig. 8 Energy minimized structure of **ZnPc3** and its adduct (1:1) with TNP optimized at B3LYP/6-31g* basis set. The Figure also depicts the electron density profiles of HOMO and LUMO orbitals of **ZnPc3** and **ZnPc3•TNP**.

The representative optimized structures of **ZnPc3** and of the adduct with TNP are shown in Fig. 8, alongside with their frontier molecular orbital electron density profiles. The HOMO orbitals of **ZnPcs** are centred on the phthalocyanine core with substantial contribution being observed from the dimethylamine groups. The LUMO energy levels are double degenerate with only one of the states shown for each system. The calculated LUMO energy levels of the **ZnPcs** are very close to the experimental ones determined from the cyclic voltammetry measurements. The HOMO-LUMO gap was found to decrease with the increase in the number of dimethylamine groups showing 2.02 eV, 2.03 eV and 1.90 eV for **ZnPc1**, **ZnPc2** and **ZnPc3**, respectively. The decrease in the HOMO−LUMO gap for **ZnPc3** arises due to a considerable

electronic coupling between the donor part of the dimethylamine groups and the phthalocyanine core. These results are in agreement with the HOMO−LUMO gap obtained from absorption and electrochemical studies. The LUMO energy level of **ZnPc3** is close to the LUMO energy level of TNP results efficient electron transfer process for high selectivity. The calculated binding energy (ΔE) of **ZnPc3** with TNP is 31132.01 kcal/mole, a value higher than the corresponding binding energies of **ZnPc1** and **ZnPc2** with TNP by 122.12 kcal/mole and 98.32 kcal/mole, respectively. The HOMO-LUMO gap of **ZnPc3** decreases significantly to 0.25 eV upon binding to TNP, whereas for **ZnPc1** and **ZnPc2** the HOMO-LUMO gap is 0.81 eV and 0.64 eV. In this context, the higher decrease in the HOMO–LUMO energy difference of **ZnPc3** pointed out to the formation of a strong charge transfer complex with TNP, with this assumption being consistent with the fluorescence quenching experiments undertaken. The frontier molecular orbitals of the **ZnPc3·TNP** adduct show that the electron density of the HOMO orbital is localized on the phthalocyanine ring while the LUMO orbitals are instead localized on the TNP molecules. This indicates that an efficient electron transfer process occurs by excited-state electron transfer from the lower lying LUMO level of **ZnPcs** to the LUMO of TNP. Similar results were obtained for other **ZnPcs** treated with TNP.
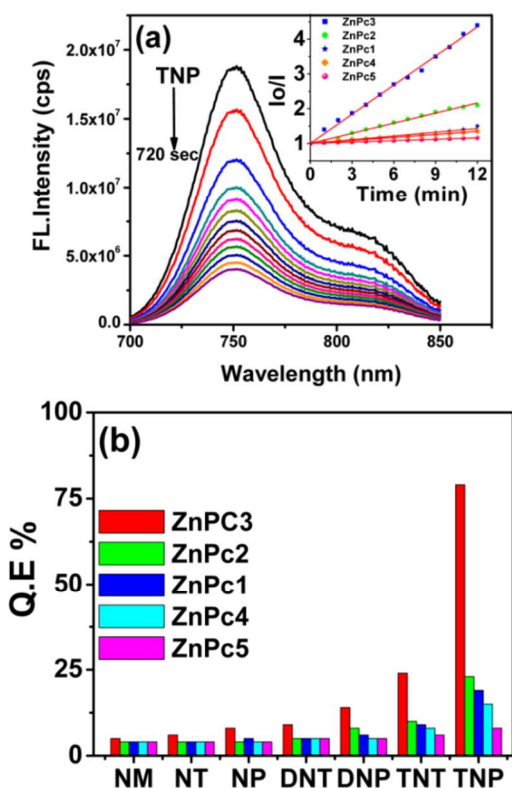
Fig. 9 (a) Time dependent fluorescence quenching of **ZnPc3** thin film upon exposure to the saturated vapours of TNP (7.7×10^{-3} ppb). The inset shows the variation in the Stern-Volmer plot of **ZnPc1-5** to the saturated vapours of TNP at different time intervals. (b) Variation in the quenching efficiency of **ZnPc1-5** to the saturated vapours of different NACs for a total exposure of 10 min.

Towards the practical use of **ZnPcs** as potential chemosensors, thin films were prepared by spin coating on a quartz substrate with a rate of 2000 rpm and a solution with concentration of 0.5 mg/0.2 mL in chloroform. The obtained thin films were annealed at 50 °C for 2 h. The absorption spectra of **ZnPcs** thin films show broaden Soret and Q-bands. The emission spectra of the thin films further depict similar

behaviour as that of the solution spectra (Fig. S36, ESI†). Solid-state fluorescence quenching of the prepared thin films was obtained by exposing them to saturated vapours of NACs over time. **ZnPc3** is highly sensitive towards the saturated vapours of TNP when compared with the same results for other **ZnPc** films. A high quenching response (76%) was obtained for 720 seconds of exposure time. Interestingly, **ZnPc4** show only 5-15% decrease in the fluorescence emission intensity. To understand the role of electron donating groups contributing to the enhanced sensitivity, fluorescence quenching studies were carried out with **ZnPc5** under similar conditions. The thin film of **ZnPc5** only showed 8% decrease in the fluorescence quenching for TNP vapours at 600 sec of exposure time. Fig. 9 shows that **ZnPc3** is highly selective towards TNP while other **ZnPcs** only show a 5-21% of decrease in the quenching efficiency; the order of reactivity is as follows: **ZnPc3**> **ZnPc2**> **ZnPc1**> **ZnPc4**> **ZnPc5**. Fig. S37 and S38 (in the ESI†) show the fluorescence quenching behaviour of **ZnPc1-5** towards saturated vapours of other NACs. The decrease in fluorescence intensity of thin films of **ZnPcs** upon exposure to the nitroaromatic vapours is ascribed to the charge-transfer complex formation between the electron rich phthalocyanines to the electron-deficient nitroaromatics through strong intermolecular interactions. In addition, steric effects may also influence the sensor behaviour. Therefore, morphological studies of the thin films were carried out with field emission scanning electron microscope (FE-SEM) to investigate structural integrity and homogeneity (Fig. 10). The samples for SEM were prepared by depositing the solutions of **ZnPcs** onto a SiO₂/Si substrate (1x1 cm²).
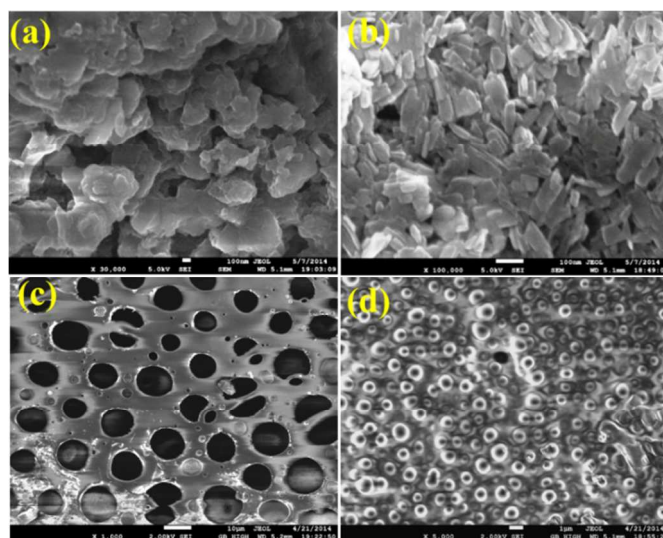
Fig. 10 Scanning electron microscope (SEM) images of **ZnPc** thin films prepared from chloroform: (a) **ZnPc1** (b) **ZnPc2** and (c) **ZnPc3**. (d) SEM of **ZnPc3** thin films obtained from methanol.

The morphology of the **ZnPc3** thin films obtained from chloroform exhibit highly ordered porous nature with variation in the pore size. The **ZnPc1** film shows cluster of aggregates and that of **ZnPc2** a more ordered crystalline morphology. In general, the formation of such porous structures for thin films were typically obtained from carbon-rich materials, polymers and other inorganic materials.[45] The formation of such morphology for phthalocyanines is, to the best of our knowledge, rare opening interesting possibilities for optoelectronic applications. We note that the morphology of the

thin films was largely influenced by the solvent employed. **ZnPc3** shows porous structures when dichloromethane and chloroform are used, while employing instead methanol promotes the formation of spherical aggregates (Fig. 10d).

The use of mixed solvents such as dichloromethane-hexane and dichloromethane-methanol, promotes the collapse of the porous film morphology with the formation of spherical crystallites. This is a clear indication that the solvent polarity plays an important role to obtain the desired porous morphology (Fig. S39, ESI[†]). **ZnPc1** and **ZnPc2** also promote the formation of spherical crystalline morphologies in methanol and in mixed solvents. The morphological results of the thin films ascribe the variation in the sensing behaviour of the different molecular structures. For example, the **ZnPc3** thin film obtained from methanol shows only 46% quenching of fluorescence for TNP vapour. It is worthy of noting that the highly ordered porous structure of **ZnPc3** can easily allow the diffusion of the vapours of NACs which, in turn, has a direct consequence in the observed selectivity and efficient binding of TNP.
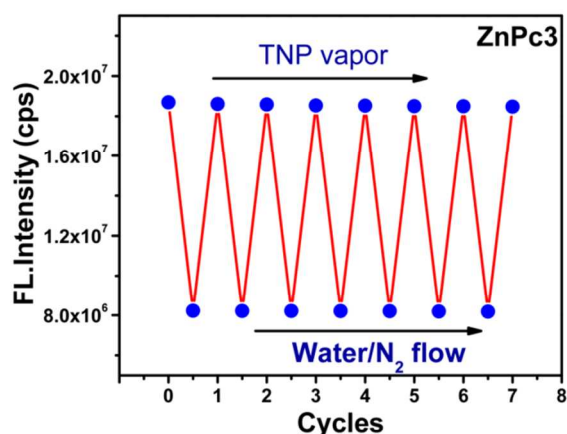
Fig. 11 Reversibility of the **ZnPc3** thin film exposed to the saturated vapours of TNP.

An important consideration to design a real time, practical, and reusable sensor is the ability to release the analyte vapours after the exposure and quickly recovery the fluorescence emission of the films. There are, nevertheless, only a handful of reports that show the recovery of the fluorescence after exposure to the analyte vapour, which may be due to the fact that recovery is often a slow process.[46] Fig. 11 shows the reversibility of the **ZnPc3** film towards the exposure of TNP vapours. The film was exposed to saturated vapours of TNP at ambient temperature for 300 s. The emission spectrum of the film was collected through front face technique and compared with the emission spectrum of the virgin film. The thin film was washed with water and dried under nitrogen flow and the emission spectrum was recorded and the whole process was repeated. The results show that the initial fluorescence intensity was significantly retained after several cycles, ultimately confirming the high photostability of the fabricated thin film.

4.Conclusions

In conclusion, we have developed a novel method for the selective substitution of dimethylamine derivatives on phthalonitriles. Cyclic tetramerization of dimethylamine phthalonitriles with $ZnCl_2$ in 1-chloronaphthalene at 200 °C forms Zn(II)phthalocyanines in 65±3% yield. It was found that increasing the number of dimethylamine groups at the peripheral positions decreases the HOMO-LUMO gap. The absorption spectra of **ZnPc1-3** in aprotic solvents exhibits a typical behaviour of monomeric form and the observed variation in the Q-band position is mainly due to solvent permittivity. In methanol, compounds show strong intermolecular aggregation with the propensity to aggregate decreasing with the increase of the alkyl chain length of the employed solvent (from methanol to octanol). We further found that the choice of the solvent has a strong impact on the observed photophysical properties, being observed a correlation between the fluorescence quantum yield and the extent of aggregation. We successfully demonstrated that **ZnPc** derivatives endowed with both electron rich and electron deficient compounds at the periphery show selective detection towards TNP. **ZnPc3** exhibits, furthermore, an efficient fluorescent chemosensor-type behaviour for TNP with a rate constant of $K_{sv}= 2.99\times10^4\,M^{-1}$ with LOD of 11±2 ppm. The order of reactivity was found to be **ZnPc3**>**ZnPc2**>**ZnPc1**>**ZnPc4**>**ZnPc5**. Time-resolved fluorescence emission and UV-Visible titration studies reveal that a static quenching phenomena is predominant by axial coordination of TNP molecules to **ZnPcs** derivatives, and also with the formation of strong inter-molecular π-π interactions. DFT studies indicate that the electron transfer occurs from the photo-excited **ZnPcs** to the electron deficient NACs. The solid state fluorescence of **ZnPc3** thin films with a typical honeycomb pore distribution exhibits 76% of quenching efficiency in 720 sec towards saturated vapours of TNP. The pore distribution for the **ZnPc3** thin films seems to enhance the diffusion of saturated vapours of TNP, ultimately leading to the observed high selectivity. The high reversibility and photostability of **ZnPc3** film demonstrating promising practical application potential in solid state sensors for selective detection of TNP.

Acknowledgements

Notes and references

[a]QOPNA and Department of Chemistry, University of Aveiro, 3810-193 Aveiro, Portugal. E-mail: jtome@ua.pt; Fax: +351 234370084; Tel: +351 234370342.

[b]CICECO and Department of Chemistry, University of Aveiro, 3810-193 Aveiro, Portugal. E-mail: filipe.paz@ua.pt; Fax: +351 234 401470; Tel: +351 234401418.

[c]Division of Chemistry and Biological Chemistry, School of Physical and Mathematical Sciences, Nanyang Technological University, Singapore 637371.

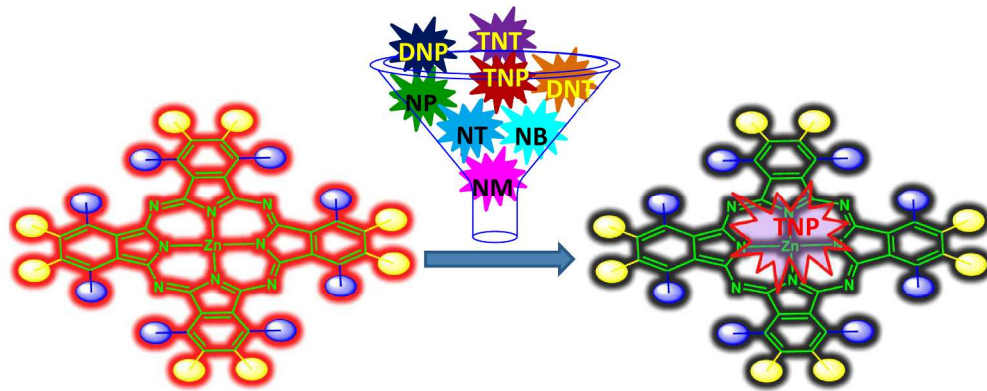[d]Department of Organic and Macromolecular Chemistry, Ghent University, B-9000 Gent, Belgium.

mm^3. Of a total of 13052 reflections collected, 1636 were independent (R_{int} = 0.0774). Final $R1$ = 0.0553 [$I > 2\sigma(I)$] and w$R2$ = 0.1244 (all data). Data completeness to theta = 25.24°, 98.5%. CCDC 1023883.

Crystal data for **2**: $C_{10}H_8ClN_3$, M = 205.64, triclinic, space group P-1, Z = 2, a = 7.0606(4) Å, b = 7.0918(4) Å, c = 10.4983(6) Å, α = 76.075(3)°, β = 71.330(3)°, γ = 77.999(3)°, V = 478.45(5) Å^3, μ(Mo-Kα) = 0.358 mm^{-1}, D_c = 1.427 g cm^{-3}, colourless block, crystal size of 0.19×0.18×0.04 mm^3. Of a total of 16051 reflections collected, 2568 were independent (R_{int} = 0.0254). Final $R1$ = 0.0345 [$I > 2\sigma(I)$] and w$R2$ = 0.0897 (all data). Data completeness to theta = 25.24°, 99.7%. CCDC 1023884.

Crystal data for **3**: $C_{12}H_{12}F_2N_4$, M = 250.26, monoclinic, space group $P2_1/n$, Z = 4, a = 6.7161(18) Å, b = 16.551(5) Å, c = 11.136(3) Å, β = 92.593(10)°, V = 1236.6(6) Å^3, μ(Mo-Kα) = 0.106 mm^{-1}, D_c = 1.344 g cm^{-3}, yellow needle, crystal size of 0.08×0.08×0.05 mm^3. Of a total of 8683 reflections collected, 2250 were independent (R_{int} = 0.0661). Final $R1$ = 0.0616 [$I > 2\sigma(I)$] and w$R2$ = 0.1771 (all data). Data completeness to theta = 25.24°, 99.6%. CCDC 1023885.

1   The Porphyrin Handbook, ed. K. M. Kadish, K. M. Smith and R. Guilard, Academic Press, San Diego, United States, 2003;

2   (a) Handbook of Porphyrin Science, ed. K. M. Kadish, K. M. Smith and R. Guilard, World Scientific Publishing, Singapore, 2010. (b) N. Venkatramaiah, B. Ramakrishna,a R. Venkatesan,a F. A. Almeida Paz and J. P. C. Tomé, *New J. Chem.*, 2013, **37**, 3745-3754.

3   I. López-Duarte, M. Wang, R. Humphry-Baker, M. Ince, M. V. Martínez-Díez, M. K. Nazeeruddin, T. Torres and M. Grätzel, *Angew. Chem. Int. Ed.*, 2012, **51**, 1895–1898.

4   L. M. O. Lourenço, M. G. P. M. S. Neves, J. A. S. Cavaleiro and J. P. C. Tomé, *Tetrahedron*, 2014, **70**, 2681–2698.

5   F. Figueira, P. M. R. Pereira, S. Silva, J. A. S. Cavaleiro and J. P. C. Tomé, *Curr. Org. Syn.*, 2014, **11**, 110–126.

6   L. M. O. Lourenço, P. M. R. Pereira, E. Maciel, M. Válega, F. M. J. Domingues, M. R. M. Domingues, M. G. P. M. S. Neves, J. A. S. Cavaleiro, R. Fernandes and J. P. C. Tomé, *Chem. Comm.*, 2014,**50**, 8363-8366.

7   Y. Gao, Y. Chen, R. Li, Y. Bian, X. Li, J. Jiang, *Chem. Eur. J.*, 2009, **15**, 13241–1325.

8   T. V. Dubinina, K. V. Paramonova, S. A. Trashin, N. E. Borisova, L. G. Tomilova and N. S. Zefirov, *Dalton Trans.*, 2014, **43**, 2799–2809.

9   D. K. P. Ng and J. Jiang, *Chem. Soc. Rev.*, 1997, **26**, 433–442.

10 A. S. Başak, A. Riza Özkaya, A. Altındal, B. Salih, A. Şengül and Ö. Bekaroğlu, *Dalton Trans.*, 2014, **43**, 5858–5870.

11 S. Silva, P. M. R. Pereira, P. Silva, F. A. A. Paz, M. A. F. Faustino, J. A. S. Cavaleiro and J. P. C. Tomé, *Chem.Comm.*, 2012, **48**, 3608–3610.

12 J. B. Pereira, E. F. A. Carvalho, M. A. F. Faustino, M. G. P. M. S. Neves, J. A. S. Cavaleiro, A. Cunha, A. Almeida and J. P.C. Tomé, *Photochem. Photobiol.*, 2012, **88**, 537–547.

13 D. D. Erbahara, I. Gürola, G. Gümüşa, E. Musluoğlua, Z. Z. Öztürka, V. Ahsena and M. Harbecka, *Sensors and Actuators B.,* 2012, *173*, 562–568.

14 J. Spadavecchia, G. Ciccarella, T. Stomeo, R. Rella, S. Capone and P. Siciliano, *Chem. Mater.*, 2004, **16**, 2083–2090.

15 C. Yuquan, Z. Wuming and L. Guang, *Sensors and Actuators B.,*1994, **2-3**, 247–249.

16 C. Pal, A. K. Sharma, A. N. Cammidge, M. J. Cook, and A. K. Ray, *J. Phys. Chem. B*, 2013, **117**, 15033–15040.

17 S. Pochekailova, J. Nožára, S. Nešpůreka, J. Rakušand and M. Karáskovád, *Sensors and Actuators B.,* 2012, **169**, 1–9.

18 X. Zhou, X. Wang, B. Wang, Z. Chen, C. He and Y. Wu, *Sensors and Actuators B.,* 2014, **193**, 340–348.

19 M. S. Rodríguez-Morgade, M. Planells, T. Torres, P. Ballester and E. Palomares, *J. Mater. Chem.*, 2008, **18**, 176–181.

20 J. M. M. Rodrigues, A. S. F. Farinha, P. V. Muteto, S. M. Woranovicz-Barreira, F. A. A. Paz, M. G. P. M. S. Neves, J. A. S. Cavaleiro, A. C. Tomé, M. T. S. R. Gomes, J. L. Sessler and J. P. C. Tomé, *Chem. Commun.*, 2014, **50**, 1359–1361.

21 A. S. F. Farinha, M. J. F. Calvete, F. A. A. Paz, A. C. Tomé, J. A. S. Cavaleiro, J. L. Sessler and J. P. C. Tomé, *Sensors and Actuators B.,* 2014, **201**, 387–394.

22 X. Liu, C. Qi, T. Bing, X. Cheng and D. Shangguan, *Anal. Chem.*, 2009, **81**, 3699–3704.

23 Y. Çağlar, N. Gümrükçüoğlu, E. Tuğba Saka, M. Ocak, H. Kantekin and Ü. Ocak, *J. Incl. Phenom. Macrocycl. Chem.*, 2012, **72**, 443–447.

24 F. D'Souza and O. Ito, *Coord. Chem. Rev.*, 2005, **249**, 1410–1422.

25 N. Venkatramaiah, S. Kumar and S. Patil, *Chem. Commun.*, 2012, **48**, 5007–5009.

26 N. Venkatramaiah, S. Kumar and S. Patil, *Chem. Eur. J.*, 2012, **12**, 14745–1451.

27 D. T. McQuade, A. E. Pullen and T. M. Swager, *Chem. Rev.*, 2000, **100**, 2537–2574.

28 F. I. Bohrer, C. N. Colesniuc, J. Park, I. K. Schuller, A. C. Kummel and W. C. Trogler, *J. Am. Chem. Soc.*, 2008, **130**, 3712–3713.

29 T. A. P. Rocha-Santos, M. T. S. R. Gomes, A. C. Duarte and J. A. B. P. Oliveira, *Talanta*, 2000, **51**, 1149–1153.

30 R. Zugle and T. Nyokong, *J. Mol. Cat: A.*, 2012, **358**, 49– 57.

31 S. W. Thomas III, G. D. Joly and T. M. Swager, *Chem. Rev.*, 2007, **107**, 1339–1386.

32 M. J. Frisch, G. W. Trucks, H. B. Schlegel, G. E. Scuseria, M. A. Robb, J. R. Cheeseman, J. A. Montgomery, Jr., T. Vreven, K. N. Kudin, J. C. Burant. et.al, Gaussian 03, Revision B.05, Gaussian, Inc., Wallingford CT, 2004.

33 J. Muzart, *Tetrahedron*, 2009, **65**, 8313–8323.

34 R. Ashokkumar, A. Kathiravan and P. Ramamurthy, *Phys. Chem. Chem. Phys.*, 2014, **16**, 1015–1021.

35 M. Kasha, *Radiation Research*, 1963, **20**, 55–71.

36 A. Ogunsipe, J. Y. Chen and T. Nyokong, *New J. Chem.*, 2004, **28**, 822–827.

37 (a) K. K. Kartha, S. S. Babu, S. Srinivasan, and A. Ajayaghosh, *J. Am. Chem. Soc.*, 2012, **134**, 4834–4841. (b) K. K. Kartha, A. Sandeep, V. C. Nair, M. Takeuchi and A. Ajayaghosh, Phys. Chem. Chem. Phys., 2014,16, 18896-18901.

38 D. Banerjee, Z. Hu and J. Li, *Dalton Trans.*, 2014, **43**, 10668–10685.

39 (a) N. Venkatramaiah, S. Kumar, and S. Patil, *Chem. Commun.*, 2012, 48, 5007–5009. (b) N. Venkatramaiah, S. Kumar and S. Patil, Chem. Eur. J., 2012, **12**, 14745–14751. (c) S. Kumar, N. Venkatramaiah and S. Patil, *J. Phys. Chem. C.*, 2013, **117**, 7236–7245.

40 N. Venkatramaiah, A. D. G. Firmino, F. A. A. Paz and J. P. C. Tomé, *Chem. Commun.*, 2014, **50**, 9683.

41 A. Rana and P. K. Panda, *RSC Adv.*, 2012, **2**, 12164–12168.

42 S. Tao, G. Li and Hesun Zhu, *J. Mater. Chem.*, 2006, **16**, 4521–4528.

43 H. A. Benesi and J. H. Hildebrand, *J. Am. Chem. Soc.*, 1949, **71**, 2703–2707.

44 D. A. S. Filho, V. Coropceanu, N. E. Gruhn, P. H. Oliveira Neto and J. Luc Bredas, *Chem. Commun.*, 2013, **49**, 6069-6071.

45 K. Cui, T. Chiba, S. Omiya, T. Thurakitseree, P. Zhao, S. Fujii, H. Kataura, E. Einarsson, S. Chiashi and S. Maruyama, *J. Phys. Chem. Lett.,* 2013, **4**, 2571−2576.

46 P. H. Ma, R. Gao, D. Yan, J. Zhao and M. Wei, *J. Mater. Chem. C*, 2013, **1**, 4128-4137.

229x89mm (300 x 300 DPI)